Lattice dynamics in perovskite halides CsSnX_{3} with X=I, Br, Cl

Ling-yi Huang and Walter R. L. Lambrecht

Phys. Rev. B **90**, 195201 — Published 5 November 2014

DOI: 10.1103/PhysRevB.90.195201

Lattice dynamics in perovskite halides $CsSnX_3$ with X=I, Br, Cl

Ling-yi Huang and Walter R. L. Lambrecht
Department of Physics, Case Western Reserve University, Cleveland, OH 44106-7079

The first-principles linear response method is used within the local-density approximation (LDA) to calculate the full phonon band structures and phonon density of states (DOS) of $CsSnX_3$ (X=Cl, Br, or I) in different phases. The relations between soft phonon modes and phase transitions are investigated. We find soft phonon modes only in the cubic and tetragonal phases, not in the orthorhombic and monoclinic phases. A dispersion-less soft phonon branch spreads from the **k**-point M to R in the Brillouin zone of the cubic phase. The lower symmetry tetragonal phase results from the condensation of the soft phonon mode at the **k**-point M. Furthermore, the condensation of the soft phonon mode at the **k**-point Z in the Brillouin zone of tetragonal phase results in the orthorhombic γ-phase. To facilitate comparison with experimental data, we calculate infrared spectra for the cubic phase. At this point only a limited comparison with experimental data is possible. We find that the calculated modes agree with the available experimental data when we assign the second and third calculated modes to the experimental first and second modes. The lowest calculated mode is at a frequency where the phonon DOS has a maximum value. So the strong phonon-phonon interaction results in short phonon lifetime or strong broadening which could explain why this mode has not been observed. Our first-principles calculated IR spectra show that the third observed mode in IR absorption is actually the highest LO rather than TO mode. We show furthermore that a strong LO-plasmon coupling may be expected in these materials and can explain observed Raman data for $CsSnI_3$.

PACS numbers: 63.20.dk,78.30.Hv

I. INTRODUCTION

Halide perovskites of the general formula ABX_3 with B standing for Sn or Pb, X a halogen (I, Br, Cl) and A a large cation such as Cs^{+1} or an organic ion such as methylammonium ($CH_3NH_3^{+1}$), have recently attracted a great deal of attention for their potential applications in solar cells.[1–13] Up to 15 % energy conversion efficiencies have been realized using these materials in the last year in a rapid development of different solar cell designs.[4,8,10,14] As the underlying reasons for this success are not yet fully understood, and further improvements appear possible, it is important to gain a better understanding of the remarkable combination of properties in this family of materials. Part of their appeal is that they are solution process-able and have tunable band gaps in the optimal range for solar cells (1.3-1.6 eV). They are excellent light absorbers in most of the visible range and also have high hole mobility and long mean free paths for both electrons and holes.

In a recent paper,[15] we discussed the electronic band structure of the $CsSnX_3$ sub-family of these materials and pointed out their "inverted" band structure, i.e. unlike most conventional semiconductors, their valence band has a strong Sn-s like character (antibondingly mixed with X-p) while their conduction band has Sn-p character. This unusual band structure already explains a number of their unusual properties, such as anomalous temperature dependence of the gap and high hole mobility. The largely intra-atomic nature of the gap explains the strong optical transitions both in luminescence and absorption. As discussed in our previous paper, however, the strong photoluminescence well separated from the absorption appears to be from a defect bound exciton rather than free exciton. As part of our study of the exciton binding energy, we needed to estimate the phonon contribution to the dielectric screening. In this paper we provide a more complete account of the lattice dynamical properties of these materials.

There are a few reasons for our interests in the phonons. First, our previous calculations of the phonon frequencies at Γ for the cubic perovskites (the so-called α-phase) only agreed with experimentally reported values after we identified our second and third highest modes with the lowest (and second) experimentally observed mode, leaving the question open, why was the lowest mode not observed? Also, what is the nature of the third observed mode which was higher than our calculated highest one? In our previous paper, we tentatively assigned it to a second harmonic but as we will show below, this assignment needs to be revised. It is in fact an LO rather than TO mode. It should be mentioned here that the only experimental paper on the vibrational infrared spectra of $CsSnBr_3$ and $CsSnCl_3$ only had a table of values in it, but no actual figures of the absorption spectra on which these values were based. For $CsSnI_3$, on the other hand, we found that the highest LO mode was assigned to a weak observed peak in Raman spectroscopy,[16] even though this mode is not Raman active to first order. In other words it is a forbidden LO mode, enhanced by resonant Raman effects. In this paper we analyze in more detail what the predicted IR phonon spectra should look like and how to reconcile these sparse experimental data with our calculated results. We will show that the LO-mode observed in Raman in fact is strongly affected by LO-plasmon coupling.

Secondly, these perovskites are known to undergo a number of phase transitions as function of temperature.[2,17–20] The cubic phase is only stable at high temperature and at lower temperature they undergo a series of transitions, corresponding to rotations and rearrangements of the octahedral SnX_6 building blocks. As discussed in detail by Chung et al.[2] in the $CsSnI_3$ case, from high temperature to low temperature, $CsSnI_3$ changes from cubic (α) phase to the tetragonal (β) phase at around 431.5±5.7 K, and then to the orthorhombic (γ) phase at around 352±5.3 K. Exposure to air (at room temperature in 1 hour) causes a transition to another orthorhombic yellow (Y) phase. As for $CsSnBr_3$, the only commonly confirmed transition is the transition from cubic (α) phase to tetragonal (β) phase, which occurs at around 292 K[18,21,22]. A second transition to another tetragonal phase was found by Mori and Saito[18] at 274 K and a transition to a monoclinic phase at 247 K. For CsSnCl3, the cubic (α) phase converts to a monoclinic (M) phase at around 363 K[21,23].

Some of these transitions are well known to be related to soft modes[18,24–28] and thus we investigate here whether soft modes occur and how these transitions relate to the soft mode displacement patterns. To this end, we need calculations of the full dispersion curves of the phonon modes. These transitions may turn out to be quite important for the durability of the new solar cell materials. In fact, some of the phase transition correspond to a more severe change in the lattice structure, in which the basic BX_6 octahedral units of the structure change from corner-sharing to side-sharing. As we already showed in our previous paper[15], this leads to a large increase in the gap making the materials far less useful for photovoltaics. The key question then becomes, how to avoid these latter phase transformations. A better understanding of the stability of the various phases with respect to soft modes is required to address this question. While we are not able at this point to provide a full understanding of the transition to the so-called yellow phase of $CsSnI_3$ and the monoclinic phase of $CsSnCl_3$, we find that the γ-phase has no soft modes and is thus mechanically stable. The transitions to the undesirable phases (from a photovoltaics point of view) appears to require more complex re-arrangements and bond breaking and reforming. In order to design better future materials in this family, it is also important to understand their trends with different constituent ion sizes. Indeed the series of phase transitions in $CsSnI_3$ appears to generally lead to a densification of the crystal structure and hence ion sizes play a key role.

The paper is organized as follows. In Section II we give details of the computational method. In section III A, we present the phonon dispersion curves and densities of states (DOS) and discuss the relation to the phase transitions. In section III B, we present our predicted IR spectra and discuss the available experimental data. In section III C, we discuss the Raman data on $CsSnI_3$ and the plasmon-LO phonon coupling.

II. COMPUTATIONAL METHOD

To calculate phonon band structures and IR spectra, we adopt the density functional perturbation theory (DFPT)[29,30] within the local density approximation (LDA). The ABINIT code[31] with norm-conserving pseudo-potentials[32] was used for these calculations. The crystal structures are first fully relaxed with respect to the lattice constants and internal parameters. The force constants and Born effective charges are then calculated from the first order corrections to the wave functions within the linear response regime in response to atomic displacements and static electric fields. The linear response formalisms allows us to obtain the dynamical matrix at arbitrary $\mathbf{k}$ point and also to obtain the non-analytic behavior at $\mathbf{k} \to 0$, i.e. the LO–TO splitting. Thus we can generate the phonon band structure throughout the Brillouin zone. We use the usual approach of Fourier interpolation of the dynamical matrix from a relatively coarse mesh ($4 \times 4 \times 4$) to the points required along symmetry lines for the sake of efficiency. For the phonon density of states, interpolation to a fine mesh of $240 \times 240 \times 240$ is used. Finally, from the Born effective charges and normal mode eigenvectors at Γ, we extract the matrix elements for the infrared spectra.

The phonon band structure calculations are expensive calculations, especially for the lower symmetry phases which have larger unit cells. We, therefore, used a $4\times4\times4$ $\mathbf{k}$-point grids for every phase. Actually, we checked the convergence of the $\mathbf{k}$-point grid for the higher symmetry phases. Although small shifts in phonon-frequencies occur the qualitative conclusions about soft-modes and the nature of the IR spectra were not affected by our choice of a relatively coarse $\mathbf{k}$-point mesh. For α-$CsSnI_3$, the highest phonon frequency at the $\mathbf{k}$-point Γ, the T^3_{1u}(LO) phonon mode which is the one we are mostly interested in, is 152 cm^{-1} for the $4\times4\times4$ k-point grid, 151 cm^{-1} for the $6\times6\times6$ k-point grid, and 148 cm^{-1} for the $8\times8\times8$ k-point grid. Our convergence studies show that the plane wave cut-off energy of about 30 Hartree is good enough for each phase. In practice, we used 28 Hartree for the orthorhombic phase, 30 Hartree for monoclinic phase, 40 Hartree for the tetragonal phase, and 100 Hartree for cubic phase; the latter two high cut-off energies are not necessary but for these smaller cells, we could afford to use a higher cut-off, which can only improve the results.

III. RESULTS

A. Phonon Band structures and soft phonon modes

Figure 1 from top to bottom shows the first-principles calculated phonon band structure and phonon density of states (DOS) resolved into atomic components for α-$CsSnI_3$, β-$CsSnI_3$, γ-$CsSnI_3$ and Y-$CsSnI_3$, respectively. The notation of the $\mathbf{k}$-points is explained in Figure 6 in our previous paper[15]. Figure 2 from top to bottom

shows the phonon band structure and phonon DOS of α-$CsSnBr_3$, β-$CsSnBr_3$, and our predicted γ-$CsSnBr_3$. Fig. 3 from top to bottom shows the phonon band structure and phonon DOS of α-$CsSnCl_3$ and M-$CsSnCl_3$, respectively. We can see that in the α and β phases, imaginary frequency modes indicated as negative frequencies (soft phonon modes) occur, while in γ, Y, and M phases, no imaginary frequency modes are found. The appearance of the soft phonon modes in α and β phases reflects the instability of those crystal structures at low temperatures. We should view the high-temperature phases as being stabilized by the additional entropy related to these soft phonon mode fluctuations.

We also can see that, in all three compounds, there is a dispersion-less soft phonon branch from M to R in the Brillouin zone of the cubic phase. The question thus arises which of these soft phonons is responsible for the phase transition. The decomposition of the DOS in different atomic contributions shows that the primary contribution to the soft phonons comes from the vibrations of the halide atoms. The absolute value of the frequency of the soft phonon modes becomes larger when the halide is changed from I to Br to Cl. This reflects the fact that the lighter mass of the atom involved, the higher the absolute value of the phonon frequency . This factor can also be used to explain why the highest phonon frequency become larger when we go from $CsSnI_3$ to $CsSnBr_3$ to $CsSnCl_3$. Furthermore, this factor explains why the vibrations of Cs (heaviest atom, compared to Sn and X) atoms only contribute to lower phonon frequency modes (say, below 100 cm^{-1}), while higher phonon frequency modes (above 100 cm^{-1}) can mainly be attributed to the vibrations of relatively lighter atoms, Sn and X. In other words, the higher phonon frequency modes come from deformations of the octahedrons, not from the relative motion of the Cs atoms and the octahedrons. However, both vibrations of octahedrons and vibrations of Cs atoms contribute to lower frequency modes.

Now, let us investigate the displacement patterns of the soft modes in the α phase first. Figure 4, from left to right shows the displacement pattern of the soft phonon mode at the M point, denoted by M_2^+ (corresponding to the irreducible representation notation of the Koster-Slater tables[33] for the group D_{4h}) (also denoted by M_3, M_3^+ or M_2^+ in different literatures depending on how the irreducible representations are ordered in the character tables)[18,27,34–38], and the three-fold degenerate soft phonon modes at the R point, denoted by R_a, R_b, and R_c, respectively. We first may note that only the halide ions are moving in these modes. At the M-point $(1,1,0)\pi/a$, the motions of the atoms on opposing vertical faces are opposite and thus correspond to a rotation of the octahedron about the **c**-axis. In adjacent unit cells, in the a-b plane, the twists are opposite leading to a new tetragonal cell rotated by 45 ° and with lattice constant $a_t = \sqrt{2}a$. The motions at the R-point $(1,1,1)\pi/a$ at first may seem more complex, but this just reflects that now there is also a phase change for the

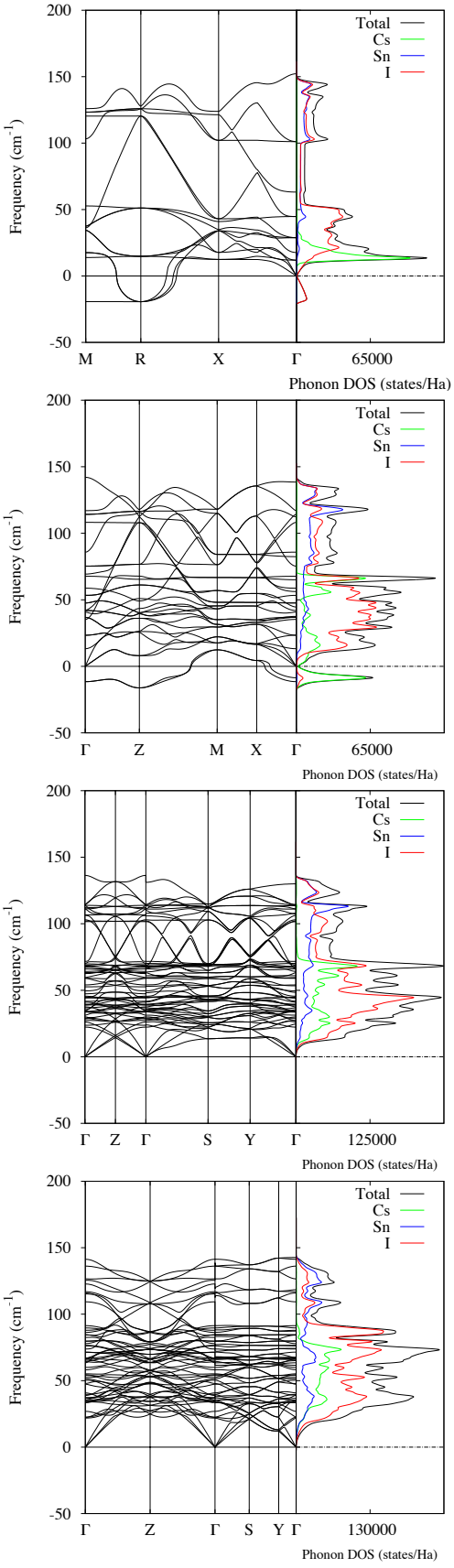

FIG. 1: Phonon band structure with phonon DOS of α-$CsSnI_3$, β-$CsSnI_3$, γ-$CsSnI_3$ and Y-$CsSnI_3$.

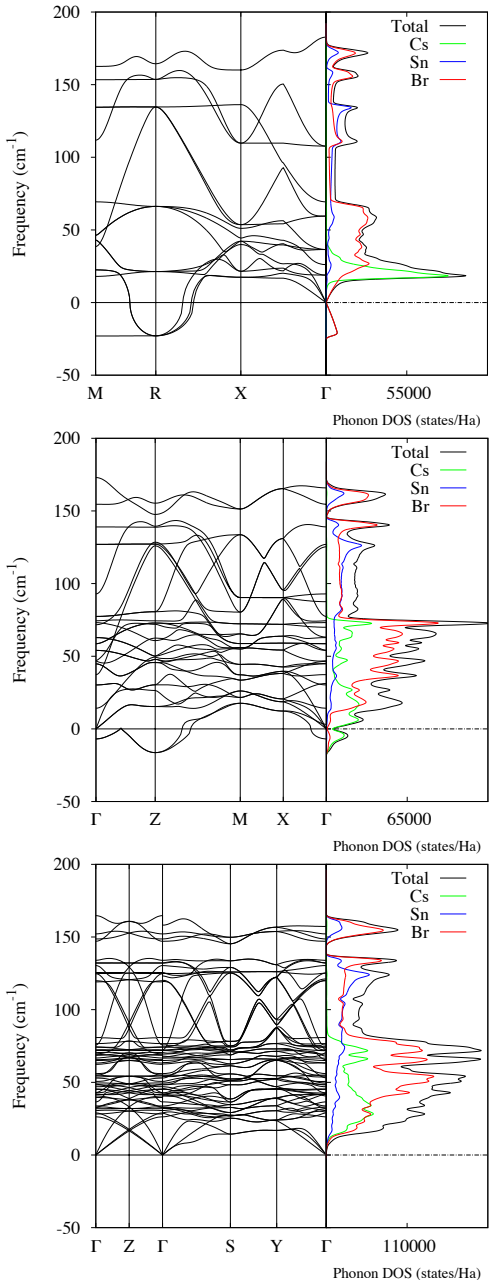

FIG. 2: Phonon band structure with phonon DOS of α-$CsSnBr_3$, β-$CsSnBr_3$, and (predict) γ-$CsSnBr_3$.

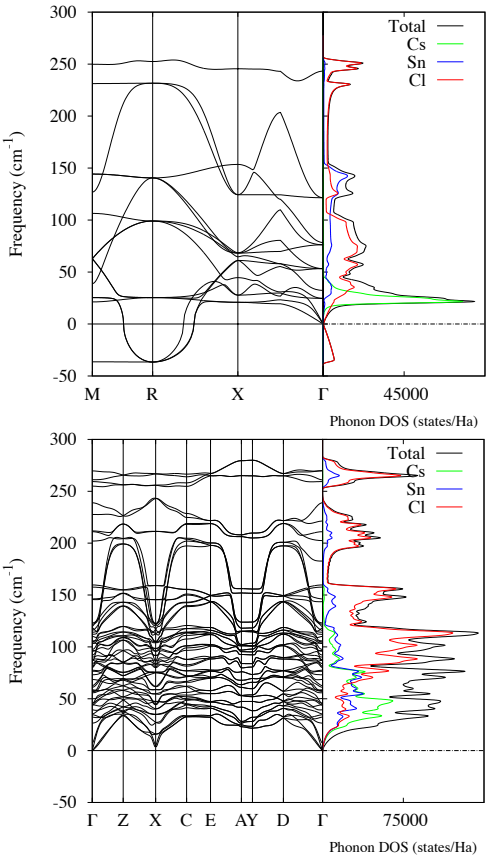

FIG. 3: Phonon band structure with phonon DOS of α-$CsSnCl_3$ and M-$CsSnCl_3$.

opposite horizontal faces. So, the rotations of the octahedron in the two unit cells stacked on top of each other are opposite and may now occur about each of the cubic axes, **a**, **b** or **c**. In the literature, these are sometimes denoted as the R_{25} mode which corresponds to the Bouckaert-Smoluchowski-Wigner[39] notation for the point group irreducible representations. It corresponds to the T_{2u} mode of the cubic group in the usual chemical notation.[40] Clearly, the $\alpha \rightarrow \beta$ phase transition corresponds to the condensation of the M_2^+ soft mode because it does not involve a doubling of the cell along the **c**-direction. This also means it corresponds to the Glazer tilt system[28,41] $a^0a^0c^+$, meaning that there is only a rotation about the **c**-axis. The R_{25} on the other hand would correspond to Glazer tilt system $a^0a^0c^-$ with alternating positive and negative twists about the c-axis.

The γ-phase is characterized by both octahedral twists about the **c**-axis and tilts about the tetragonal **a**-axis. It corresponds to the Glazer notation $a^+b^-b^-$. The R_{25} mode corresponds to only twisting about the axes but in opposite direction in alternating unit cells. The γ phase can thus not be obtained directly from the α phase. Inspection of the soft mode at the Z-point in the β-phase as shown in Fig. 5 reveals that not only the octahedrons rotate about the **b**-axis but also the Cs atoms rotate about the **a**-axis. The symmetry of this mode is Z_5^- in the Koster-Slater notation. It is doubly degenerate because one can either rotate the Cs about **a** and octahedra about **b** or vice versa.

The sequence of phase transitions can also be analyzed using group theory. The space group of the tetragonal phase (with space group No. 127 D_{4h}^5 or $P4/mbm$) is an isotropy subgroup of space group of the cubic phase (with space group No. 221 O_h^1 or $Pm\bar{3}m$). According to group theory, the space group No. 221 can go to the space group No. 127 via four transformations[38]: X_5^+, X_5^-, M_2^+, and M_3^+ (using the notation from Stokes and Hatch[38]).

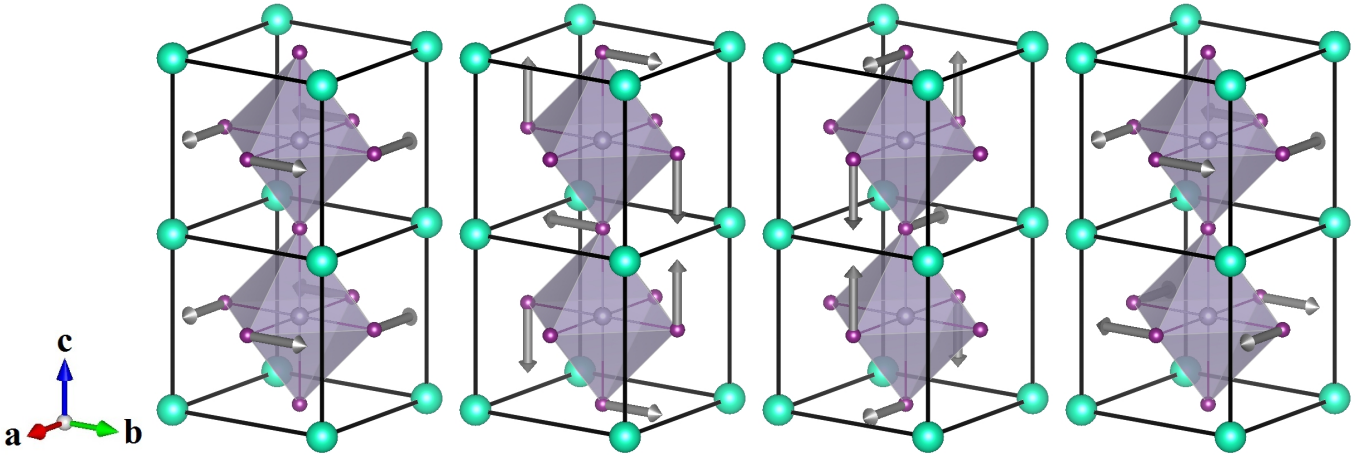

FIG. 4: From left to right shows the displacement patterns of soft phonon mode M_2^+, R_a, R_b, and R_c, or R_{25}, in the cubic phase, respectively. The green spheres are Cs atoms located at the corners of cubic unit cells, the gray ones are Sn atoms located at the center of unit cells, and the purple ones are X, X=I, Br, or Cl, located at the surface centers of unit cells. The displacements are represented by gray arrows.

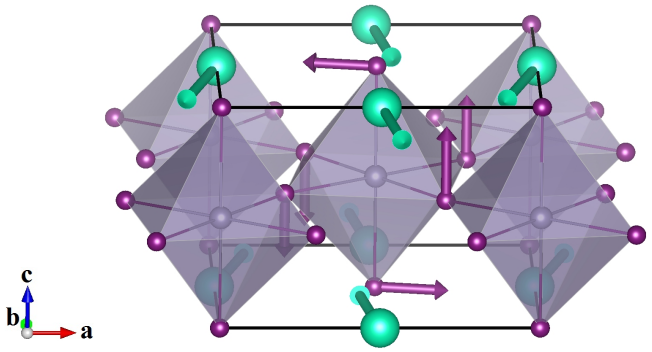

FIG. 5: The displacement pattern of the soft phonon mode at the **k**-point Z in the β-$CsSnI_3$. The green spheres are Cs atoms, the grey ones are Sn atoms, and the purple ones are I atoms. The displacements of Cs atoms are represented by green arrows, while the displacements of I atoms are represented by purple arrows. For clarity, we only show the displacements of I atoms in the central octahedron. The phonon mode is named Z_5^-.

But only the operation of M_2^+ leads to the correct atomic positions:

$$\left(\frac{x}{2}+\frac{y}{2}-\frac{1}{2},-\frac{x}{2}+\frac{y}{2},z\right) \tag{1}$$

(in reduced coordinates) in the tetragonal phase, where (x, y, z) are the reduced coordinates of an atom in the cubic phase. In fact, we may note that there is no soft phonon at the X-point the cubic BZ. In this way, the Cs atom at (0,0,0) in the cubic phase transforms to the 2d (Wyckoff) positions in the tetragonal phase. The Sn atom at (0.5,0.5,0.5) in the cubic phase transforms to the 2b (Wyckoff) positions in the tetragonal phase. Finally, the I atom at (0.5,0.5,0) in the cubic phase goes to the 2a (Wyckoff) positions in the tetragonal phase and I atoms at (0.5,0,0.5) and (0,0.5,0.5) transform to 4h (Wyckoff) positions in the tetragonal phase. So the effect of condensation of the M_2^+ soft phonon mode is equivalent to the operation described by Eq.(1) in terms of a coordinate transformation.

The same analysis can be applied to the phase transformation from the β phase to γ phase (with space group No. 62 or D_{2h}^{16} or $Pnma$). The space group No. 127 can go to the space group No. 62 via two transformation: Z_5^- and Z_5^+. But only the operation of Z_5^-:

$$(x', y', z') \to \left(y', x' - \frac{1}{2}, \frac{z'}{2} - \frac{1}{4}\right) \tag{2}$$

transforms the atoms in the β phase to the correct positions in the γ phase. (Please notice that the y-coordinate and z-coordinate are switched compared to the notation in the book of Stokes and Hatch[38].) The Cs atoms at 2d positions in the β phase transform to the 4c positions in the γ phase, the Sn atoms at the 2b positions in the β phase transform to the 4b positions in the γ phase, and the I atoms at the 2a and 4h positions in the β phase transform to the 4c and 8d positions in the γ phase, respectively. So the effect of condensation of the Z_5^- soft phonon mode is equivalent to the operation described in Equation (2) for the coordinate transformation. The phase transitions from the α phase to β phase, then to γ phase, can be summarized as follows

$$O_h^1 \xrightarrow{M_2^+} D_{4h}^5 \xrightarrow{Z_5^-} D_{2h}^{16} \tag{3}$$

In the paper by Mori and Saito[18] it was claimed that the β-$CsSnBr_3$ (with space group No. 127) can transform to the lower symmetry phase with space group No.90 (D_4^2 or $P42_12$) by the condensation of the R_{25} soft phonon mode. But from the group theory point of view, this appears incorrect. According to the group theory, the

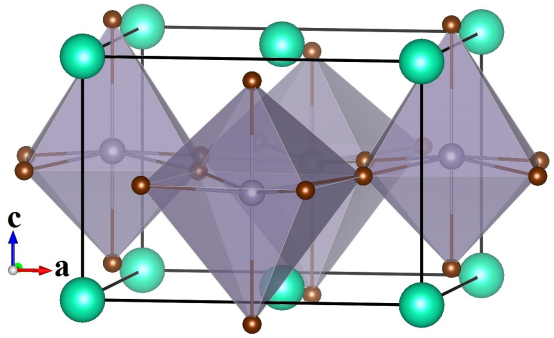

FIG. 6: The proposed crystal structure of $CsSnBr_3$ in the D_4^2 space group No. 90. The Γ_1^- deformation distorts the octahedra compared to the β-phase. The green spheres are Cs atoms, the grey ones are Sn atoms, and the brown ones are Br atoms.

space group No. 127 can only transform to the No. 90 isotropy subgroup via the operation Γ_1^-:

$$(x', y', z') \rightarrow \left(x', y' - \frac{1}{2}, z'\right). \tag{4}$$

However, as illustrated in Fig. 6, the operation of Γ_1^--symmetry is related to displacements of Sn atom and I atoms just above and below the Sn along the **c**-axis (z-direction). It is thus not related to the rotations of the R_{25} soft phonons and does not correspond to a soft mode. Also, in this space group the **c**-lattice constant is not doubled, as mentioned by Mori and Saito.[18] An R_{25} soft-mode directly from the cubic phase could lead to space group 140, D_{4h}^{18} or $I4/mcm$ instead. So, it appears that either the space-group determination or the soft mode analysis is incorrect in Ref. 18. We also note that the γ-phase has not been observed for this material but is, according to our calculations, free of soft-phonon modes and hence mechanically stable. Further work on the nature of the phase transitions in $CsSnBr_3$ appears to be necesary.

The structural changes from α to β, and to γ phases only involve the rotations (with some slight distortions) of the octahedrons; all octahedrons remain corner shared. However, the crystal structure of the yellow phase and monoclinic phase are quite different from those of the α, β, and γ phases; they display edge-sharing of the octahedra, so re-bonding is required. It seems that the phase transitions from γ-$CsSnI_3$ to Y-$CsSnI3_3$ and from α-$CsSnCl_3$ to M-$CsSnCl_3$ cannot be described by condensations of particular soft phonons. In fact, we find no soft phonon modes in the γ-phase of any of these compounds. This indicates the mechanical stability of this phase. However, this does not preclude chemically induced further phase transitions.

We finally note that the series of phase transitions from α to β to γ increase the density of the crystal. They are driven by the fact that the cage size for the Cs atom in the ideal cubic perovskite is set by the Sn-I octahedron size and is slightly too large for a Cs atom. This is related to the tolerance factor t, defined for example in Benedek and Fennie,[42] and given by

$$t = \frac{R_{AC}}{\sqrt{2}R_{BC}} \tag{5}$$

with R_{AC} and R_{BC} ideal bond-lengths. Using ideal bond-lengths based on Shannon ionic radii,[43] we obtain t-values of 0.987, 0.971 and 0.900 for the $CsSnCl_3$, $CsSnBr_3$, $CsSnI_3$ case respectively. The fact that these are smaller than 1 indicates that rotations of the octahedra are expected and is consistent with the general trend of oxide perovskites of a transition to the $Pnma$ phase group for materials with $t < 1$. The driving force for this stabilization is to optimize the environment of the A-cation. We note that for $CsSnCl_3$, with the largest t among these materials, the transitions to the β-phase and γ-phase were not observed, but instead a transition to the differently bonded monoclinic phase occurs. For the I and Br case, the rotation angles about the c-axis in the β-phase, are respectively 13.89° and 12.63° based on the calculated relaxed structures. For the γ-phase, the rotations about the c-axis and a-axis are calculated to be 13.86° and 10.23° for $CsSnI_3$ and 11.86° and 8.74° for $CsSnBr_3$. Thus, the smaller t, the larger the rotation as expected. We only have experimental values for $CsSnI_3$ where the crystal structure measured by X-ray diffraction[19] correspond to an angle of 9.09° in the β-phase and 10.09° and 3.85° in the γ-phase relative to the c and a axes respectively. The calculations agree qualitatively with the experiments in terms of order of magnitude and in predicting that the rotation about the c-axis is larger than that about the a-axis.

B. Comparison of zone center modes with experimental data

The experimental data on the phonon spectra of these materials are rather scarce. For the cubic phase, in particular, there are no allowed Raman active modes. Group theory analysis shows that there are three T_{1u} modes (IR active) and one silent T_{2u} mode at Γ. As far as infrared studies, we found only one study for α-$CsSnBr_3$ and $CsSnCl_3$.[44] Unfortunately, this paper only gives a table of the modes but shows no actual spectra. The results are said to be obtained from absorption measurements on powders. The paper does not mention anything about TO–LO splittings and since they measured absorption, one would assume that these correspond to the TO-modes. A direct comparison with our calculated results in this (as will be shown later erroneous) interpretation is shown in Table I and shows discrepancies from 50 % to 72 %.

We note that the LDA underestimate of the unit cell volume may lead to an overestimate of the phonon frequencies, in particular for bond-stretch modes. To investigate this further we have calculated the fractional change in phonon frequency per fractional change in

TABLE I: Direct (but erroneous) comparison of our calculated TO phonon frequencies (cal.) with experimental results (exp.) from Donaldson et. al.[44]. The last column gives the mode-Grüneisen parameters. All frequencies are in units of cm^{-1}.

	mode	cal.	exp.	error	γ
α-$CsSnBr_3$	T^1_{1u}(TO)	19	68	72 %	-8.6
	T^2_{1u}(TO)	59	118	50 %	0.037
	T^3_{1u}(TO)	108	218	50 %	-4.3
α-$CsSnCl_3$	T^1_{1u}(TO)	25	70	64 %	-7.7
	T^2_{1u}(TO)	76	172	56 %	0.12
	T^3_{1u}(TO)	121	310	61 %	-5.2

TABLE II: Comparison of our calculated phonon frequencies (cal.) with experimental results (exp.) from Donaldson et al.[44]. All frequencies are in units of cm^{-1}.

	mode	cal.	exp.	error
α-$CsSnBr_3$	T^1_{1u}(TO-LO)	23		
	T^2_{1u}(TO-LO)	64	68	6 %
	T^3_{1u}(TO)	108	118	8 %
	T^3_{1u}(LO)	184	218	16 %
α-$CsSnCl_3$	T^1_{1u}(TO-LO)	29		
	T^2_{1u}(TO-LO)	77	70	10 %
	T^3_{1u}(TO)	121	172	30 %
	T^3_{1u}(LO)	246	310	21 %

lattice volume, i.e. the mode-Grüneisen parameters, $\gamma_i = d\ln\omega_i/d\ln V$. These are also included in Table I. We note that correcting the volume would shift our phonon frequencies down (except for T^2_{1u}(TO) phonons), thus worsening the agreement with experiment. As already mentioned in our previous paper[15] we noted that the comparison is better between our second and third modes with their first and second modes, in particular if we average over TO and LO modes. However, this requires explaining why the first mode was not observed and what is the higher observed third mode. We already showed in our previous paper that the oscillator strength for the lowest mode is smaller than the second one by a factor 6 in $CsSnI_3$ and by a factor 4 in $CsSnBr_3$ but not in $CsSnCl_3$ where they are predicted to be about equal.

To further investigate these questions, we calculated infrared spectra even though at present we have no experimental curves to compare with. Figures 7 shows the first-principles calculated real part and imaginary part of the dielectric function, ε, the imaginary part of $-1/\varepsilon$, the absorption coefficient and the normal incidence reflectivity of α-$CsSnX_3$. As is well known, the peaks in the $\mathrm{Im}\{\varepsilon\}$ corresponds to the TO phonons while the peaks in $-\mathrm{Im}\{\varepsilon^{-1}\}$ correspond to the LO phonons. We can see that the LO–TO splitting is negligible for the lowest $T^{(1)}_{1u}$ mode, which is consistent with its weak oscillator strength. For the second mode, the LO mode shows up in the absorption curves only as a weak shoulder for $CsSnBr_3$ and as a slight asymmetry of the peak in $CsSnCl_3$. Interestingly, the LO–TO splitting of this mode is largest for $CsSnI_3$ but no IR-data are available for this material. However, the third $T^{(3)}_{1u}$ shows clearly separated LO and TO peaks in absorption. Noticing that the absorption coefficient is given by:

$$\alpha(\omega) = \frac{2\omega \mathrm{Im}\{\epsilon(\omega)\}}{n(\omega)c} \tag{6}$$

with c the speed of light, it becomes clear that the peaks in absorption can also correspond to a zero or minimum in the index of refraction $n(\omega) = \mathrm{Re}\{\sqrt{\varepsilon}\}$ and this explains the highest peak in the experimental absorption spectrum as an LO-mode. Thus it becomes clear that the three peaks observed in the experiment are respectively, the $T^{(2)}_{1u}$ mode (averaged over TO and LO), the $T^{(3)}_{1u}(TO)$ and $T^{(3)}_{1u}(LO)$ modes. The current interpretation of the highest observed mode is different from our tentative assignment in the previous paper[15] as a two phonon absorption peak. The latter tentative explanation was only based on numerical values of $2\omega_{T^{(3)}_{1u}(TO)}$ but ignores the relative probabilities of single and two-phonon absorption and the fact that two-phonon absorption would be more complex than just getting overtones of the one-phonon frequencies at Γ. We think this explanation is far less likely. Although our present interpretation does not match perfectly either, it is a more straightforward explanation.

From the Fig.7, it appears however that the $T^{(1)}_{1u}$ mode has comparable intensity in absorption to the $T^{(2)}_{1u}$ mode. However, in constructing these spectra we used the same broadening for each peak. Returning to Figs.(2,3) we can see that the lowest mode at the Γ-point coincides with a sharp peak in phonon DOS whereas the second peak lies in a region of lower density of states (especially for $CsSnBr_3$). Thus we expect strong phonon-phonon scattering (or an-harmonic effects) on this mode may lead to a short lifetime or strong broadening. This would strongly reduce the peak height and might explain why this mode was not observed in the experimental absorption spectrum.[44] We can see that this mode corresponds to an almost dispersionless band corresponding to the Cs motion relative to the SnI_6 octahedron and is dominated by the Cs motion. The final comparison with experimental data using this interpretation is shown in Table II. The maximum error is now reduced to 30% and occurs for the $T^{(3)}_{1u}(TO)$ mode of $CsSnCl_3$. The origin of this discrepancy is difficult to ascertain without reliable experimental spectra. We note that the LO-mode in both materials appears to be underestimated by our calculation. This is addressed in the next section.

C. LO-plasmon coupling effect

Although we could not find IR absorption data in the literature for $CsSnI_3$, Yu et al.[16] measured the Raman

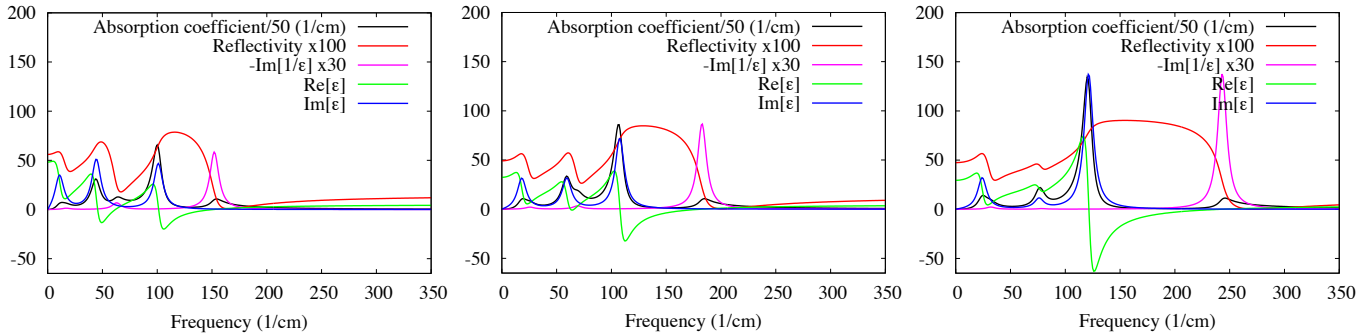

FIG. 7: The real part and imaginary part of dielectric function, ε, imaginary part of -1/ε, absorption coefficient and reflectivity of α-$CsSnI_3$ (left), α-$CsSnBr_3$ (middle) and α-$CsSnCl_3$ (right).

spectrum for γ-$CsSnI_3$. In Figure 1 of their paper, the Raman spectrum shows two peaks located at 258 and 472 cm^{-1}, respectively. They claimed the first peak is from the first-order LO phonon scattering, while the second peak is from the triply enhanced second-order Raman scatting. Although we have already mentioned that in α-$CsSnI_3$ none of the modes are Raman active, Raman active modes could exist in the γ-phase or could be observed as LO-forbidden modes[45,46] by means of the Fröhlich mechanism. This makes sense because the gap of the material is rather low, (1.3 eV) and thus the lasers used in Raman spectroscopy in Ref. 16 are above the gap which leads to resonantly enhanced Raman scattering even for the first order Raman scattering. The resonant Raman effect is well known to enhance the intensity of forbidden LO-modes. We also may note that because the β and γ phases still have an inversion center, the modes derived from the α-phase T_{1u} modes remain odd with respect to inversion and therefore Raman inactive even in the β and γ phases. The only Raman active modes in those materials will arise from new modes at the zone center arising from folded zone-edge modes.

However, with this interpretation, there appears again to be a large discrepancy between the measured value of the frequency (258 cm^{-1}) and our calculated T_{1u}^3 LO mode in $CsSnI_3$ (152 cm^{-1}). As we have seen earlier, this highest mode is not significantly shifting from the α to γ phases. The discrepancy is 41 % and thus larger than for $CsSnBr_3$ or $CsSnCl_3$ discussed in the previous section but we note that in all cases, our calculations appear to underestimate the LO-mode.

Since these materials, in particular $CsSnI_3$ are known to be rather conductive by unintentional p-type doping, we test the hypothesis that this shift could arise from LO-plasmon coupling. The plasmon frequency can be written:

$$\omega_p = \sqrt{\frac{4\pi n e^2}{m^* \varepsilon_\infty}}, \tag{7}$$

where n is the concentration of carriers, e is the electric charge, m^* is effective mass of the carrier, and ε_∞ is the high-frequency dielectric constant in the material. In the present case, the carriers are holes; we have calculated the effective mass of hole and the high-frequency dielectric constant in our previous paper[15] and obtained m^*=0.069 m_e and ε_∞=4.86 for α-$CsSnI_3$. The remaining unknown physical quantity is the concentration of holes, n. Fortunately, in the paper from Chung et al.[2], they measured the concentration of carriers and reported carrier concentration of about 10^{17} cm^{-3} for $CsSnI_3$ at room temperature. If n goes from 10^{16} to 10^{18} cm^{-3}, ω_p changes as function of $\sqrt{n}$ from 52 to 517 cm^{-1}, which is comparable to the frequency of the LO phonon modes. Thus we expect strong LO-plasmon coupling. We note that the low phonon frequencies (due to the heavy masses of the ions involved) conspire with the unusually low hole mass and low high-frequency dielectric constant in this material to produce comparable LO and plasmon frequencies even for moderate carrier concentration. We are now in a position to calculate the frequency of LO-plasmon coupled mode, denoted by ω_{LO-p}. The dielectric function in the presence of the free carriers in a semiconductor is[47]

$$\epsilon(\omega) = \epsilon_\infty \left(1 + \frac{\omega_{LO}^2 - \omega_{TO}^2}{\omega_{TO}^2 - \omega^2} - \frac{\omega_p^2}{\omega^2}\right). \tag{8}$$

By solving the equation $\epsilon(\omega)$=0, we obtain

$$\omega_{LO-p}^2 = \frac{1}{2}\left(\omega_{LO}^2 + \omega_p^2\right) \pm \left[\frac{\left(\omega_{LO}^2 + \omega_p^2\right)^2}{4} - \omega_{TO}^2 \omega_p^2\right]. \tag{9}$$

Using our calculated ω_{TO} = 101 cm^{-1} and ω_{LO} = 152 cm^{-1} and other constants as mentioned above, we find that for hole concentrations from 10^{16} to 10^{18} cm^{-3}, ω_{LO-p} varies from 157 to 530 cm^{-1}. Clearly, this range encompasses the experimental value of 258 cm^{-1}, which in this model would correspond to a plausible carrier concentration of 1.92×10^{17} cm^{-3}. In this case, the upper LO-plasmon coupled mode is more plasmon than LO-like. Unfortunately, we do not know independent measurements of the carrier concentration in the samples used in Ref. 16. Our interpretation predicts that the Ra-

man spectra could shift significantly with carrier concentration. Furthermore, In Chung et al.[2] already showed that significant changes in carrier concentration can be induced by high-temperature annealing because this creates more hole generating acceptor native defect states. We thus propose that our interpretation could be tested by measuring the Raman spectrum after annealing treatments. Obviously, the LO-plasmon coupling effect is also expected to occur in $CsSnBr_3$ and $CsSnCl_3$ and could thus also explain our underestimate of the LO mode compared to the highest observed IR absorption peak. Since the highest LO mode involved in this LO-plasmon effect is a breathing mode of the octahedra, it should also be applicable in the hybrid halide perovskites.

IV. CONCLUSIONS

In this paper, we presented full phonon band structures and atom resolved densities of states for $CsSnX_3$, X=I, Br, Cl for various structures. These calculations showed soft-phonon modes between M and R in the cubic α phase and near Z in the tetragonal β-phase. We showed that their normal mode displacement patterns correspond to a pure octahedron rotation about one cubic axis for the M point, and an alternating rotation of octahedra back and forth along one axis for the R-point. The M-rotations which correspond to the irreducible representation M_2^+ are responsible for the phase transition to the β-phase. The normal mode of the soft mode at Z, which has Z_5^- symmetry combines further rotations of the octahedrons about one axis perpendicular to the tetragonal symmetry axis and rotation of the Cs atoms about the other axis. This mode is responsible for the $\beta \rightarrow \gamma$ transition. The γ-phase is found to be mechanically stable because it displays no soft-phonon modes. We find it also to be stable in $CsSnBr_3$ and thus predict this phase might be the stable one in this material at lower temperatures. On the other hand, the yellow phase of $CsSnI_3$ and monoclinic phase of $CsSnCl_3$ involve a more complex re-arrangement of octahedra into edge-sharing octahedra, which clearly cannot be obtained from a soft-phonon mechanism. These phases themselves show no soft-phonon modes. They remain nevertheless a concern for photovoltaic applications for the ultimate stability of these materials in different chemical environments (for example moist air) because these phases have much larger band gaps.

We predicted infrared spectra from the α-phase of all three compounds, in the form of reflectivity, absorption and dielectric functions. We re-interpreted the few available experimental data on α-$CsSnBr_3$ and α-$CsSnCl_3$. The three reported experimental frequencies correspond to the $T_{1u}^{(2)}(TO-LO)$ average mode, $T_{1u}^{(3)}(TO)$ and $T_{1u}^{(3)}(LO)$ modes respectively. The lowest mode $T_{1u}^{(1)}$ at about 20-30 cm^{-1} is shown to have low oscillator strength, low LO-TO splitting and is expected to have a short lifetime due to its coincidence with a strong peak in phonon density of states which would broaden the transition to the extent that it becomes difficult or impossible to detect. It involves mostly the motion of the heavy Cs ion, which is in some sense rattling about in its too large cage. This sluggish mode is possibly of interest for thermoelectric properties because it could strongly suppress thermal conductivity. Furthermore we pointed out that in these materials a strong LO-hole-plasmon coupling can be expected because of the relatively high plasmon frequency related to the low hole mass and low high-frequency dielectric constant and low LO-phonon frequency even for moderately low carrier concentrations of order 10^{17} cm^{-3}.

Acknowledgments

This work was supported by the U.S. Department of Energy, Office of Science, Basic Energy Sciences, under Award No. ER 46874–SC0008933. The calculations used the High Performance Computing Resource in the Core Facility for Advanced Research Computing at Case Western Reserve University.

[1] I. Chung, B. Lee, J. He, R. P. H. Chang, and M. G. Kanatzidis, Nature **485**, 486 (2012).
[2] I. Chung, J.-H. Song, J. Im, J. Androulakis, C. D. Malliakas, H. Li, A. J. Freeman, J. T. Kenney, and M. G. Kanatzidis, Journal of the American Chemical Society **134**, 8579 (2012), http://pubs.acs.org/doi/pdf/10.1021/ja301539s, URL `http://pubs.acs.org/doi/abs/10.1021/ja301539s`.
[3] H.-S. Kim, C.-R. Lee, I. Jeong-Hyeok, K.-B. Lee, T. Moehl, A. Marchioro, S.-J. Moon, R. Humphry-Baker, J.-H. Yum, J. E. Moser, et al., Scientific Reports **2**, 591 (2012).
[4] J. Burschka, N. Pellet, S.-J. Moon, R. Humphry-Baker, P. Gao, M. K. Nazeeruddin, and M. Grätzel, Nature **499**, 316 (2013).
[5] M. M. Lee, J. Teuscher, T. Miyasaka, T. N. Murakami, and H. J. Snaith, Science **338**, 643 (2012).
[6] J. M. Ball, M. M. Lee, A. Hey, and H. J. Snaith, Energy Environ. Sci. **6**, 1739 (2013).
[7] G. E. Eperon, V. M. Burlakov, P. Docampo, A. Goriely, and H. J. Snaith, Advanced Functional Materials **24**, 151 (2014).
[8] M. Liu, M. B. Johnston, and H. J. Snaith, Nature **501**, 395 (2013).
[9] W. Zhang, M. Saliba, S. D. Stranks, Y. Sun, X. Shi, U. Wiesner, and H. J. Snaith, Nano. Lett. **13**, 4505 (2013).
[10] K. Wojciechowski, M. Saliba, T. Leijtens, A. Abate, and H. J. Snaith, Energy Environ. Sci. **7**, 1142 (2014).
[11] M. A. Loi and J. C. Hummelen, Nature Materials **12**, 1087

(2013).
[12] F. Brivio, K. T. Butler, A. Walsh, and M. van Schilfgaarde, Phys. Rev. B **89**, 155204 (2014), URL http://link.aps.org/doi/10.1103/PhysRevB.89.155204.
[13] J. M. Frost, K. T. Butler, F. Brivio, C. H. Hendon, M. van Schilfgaarde, and A. Walsh, Nano Letters **14**, 2584 (2014), http://pubs.acs.org/doi/pdf/10.1021/nl500390f, URL http://pubs.acs.org/doi/abs/10.1021/nl500390f.
[14] G. Hodes, Science **342**, 317 (2013).
[15] L.-y. Huang and W. R. L. Lambrecht, Phys. Rev. B **88**, 165203 (2013).
[16] C. Yu, Z. Chen, and K. Shum, Journal of Raman Spectroscopy **44**, 262 (2013), ISSN 1097-4555, URL http://dx.doi.org/10.1002/jrs.4180.
[17] S. Sharma, N. Weiden, and A. Weiss, Z. Physik. Chem. **175**, S. 63 (1992).
[18] M. Mori and H. Saito, J. Phys. C: Solid State Phys. **19**, 2391 (1986).
[19] K. Yamada, S. Funabiki, H. Horimoto, T. Matsui, T. Okuda, and S. Ichiba, Chemistry Letters **20**, 801 (1991).
[20] P. Mauersberger and F. Huber, Acta cryst. B **36**, 683 (1980).
[21] J. Barrett, S. R. A. Bird, J. D. Donaldson, and J. Silver, J. Chem. Soc. A **1971**, 3105 (1971).
[22] D. E. Scaife, P. F. Weller, and W. G. Fisher, J. Solid. State Chem. **9**, 308 (1974).
[23] F. R. Poulsen and S. E. Rasmussen, Acta Chem. Scand. **24**, 150 (1970).
[24] K. Gesi, J. D. Axe, and G. Shirane, Phys. Rev. B **5**, 1933 (1972).
[25] J. F. Scott, Reviews of Modern Physics **46**, 83 (1974).
[26] G. Shirane, Reviews of Modern Physics **46**, 437 (1974).
[27] Y. Fujii and S. Hoshino, Phys. Rev. B **9**, 4549 (1974).
[28] P. M. Woodward, Acta Cryst. **B53**, 44 (1997).
[29] X. Gonze, Phys. Rev. B **55**, 10337 (1997).
[30] X. Gonze and C. Lee, Phys. Rev. B **55**, 10355 (1997).
[31] X. Gonze, J. M. Beuken, R. Caracas, F. Detraux, M. Fuchs, G. M. Rignanese, M. Sindic, L.and Verstraete, G. Zerah, and F. Jollet, Computational Materials Science **25,3**, 478 (2002/11), URL http://www.abinit.org.
[32] C. Hartwigsen, S. Goedecker, and J. Hutter, Phys. Rev. B **58**, 3641 (1998), URL http://link.aps.org/doi/10.1103/PhysRevB.58.3641.
[33] G. F. Koster, *Properties of the thirty-two point groups* (MIT Press, Cambridge, 1963).
[34] J. Zak, *The Irreducible Representations of Space Groups* (W. A. Benjamin, New York, 1969).
[35] C. J. Bradley and A. P. Cracknell, *The Mathematical Theory of Symmetry in Solids* (Clarendon, Oxford, 1972).
[36] S. C. Miller and W. F. Love, *Tables of Irreducible Representations of Space Groups and Co-representations of Magnetic Space Groups* (Pruett, Boulder, 1967).
[37] A. P. Cracknell, B. L. Davies, S. C. Miller, and W. F. Love, *Kronecker Product Tables* (Plenum, New York, 1979).
[38] H. T. Stokes and D. M. Hatch, *Isotropy Subgroups of the 230 Crystallographic Space Groups* (World Scientific, Singapore New Jersey London Hong Kong, 1988).
[39] L. P. Bouckaert, R. Smoluchowski, and E. Wigner, Phys. Rev. **50**, 58 (1936), URL http://link.aps.org/doi/10.1103/PhysRev.50.58.
[40] M. Tinkham, *Group Theory and Quantum Mechanics* (McGraw-Hill Book Company, New York, 1964).
[41] A. M. Glazer, Acta Crystallographica Section B **28**, 3384 (1972), URL http://dx.doi.org/10.1107/S0567740872007976.
[42] N. A. Benedek and C. J. Fennie, J. Phys. Chem. C **117**, 13339 (2013), http://pubs.acs.org/doi/pdf/10.1021/jp402046t, URL http://pubs.acs.org/doi/abs/10.1021/jp402046t.
[43] R. D. Shannon, Acta Cryst. A **32**, 751 (1976), URL http://dx.doi.org/10.1107/S0567739476001551.
[44] J. D. Donaldson, S. D. Ross, and J. Silver, Spectrochimica Acta **31A** (1975).
[45] R. M. Martin and T. C. Damen, Phys. Rev. Lett. **26**, 86 (1971), URL http://link.aps.org/doi/10.1103/PhysRevLett.26.86.
[46] R. M. Martin, Phys. Rev. B **4**, 3676 (1971), URL http://link.aps.org/doi/10.1103/PhysRevB.4.3676.
[47] P. Y. Yu and M. Cardona, *Fundamentals of Semiconductors Physics and Materials Properties Fourth Edition* (Springer, Heidelberg Dordrecht London New York, 2010).